Design and Analysis of a New Drive-Integrated Auxiliary Dc-Dc Converter for Hybrid Vehicles

H. Plesko, J. Biela, and J. W. Kolar
Power Electronic Systems Laboratory, ETH Zurich
ETH-Zentrum, ETL I16, Physikstrasse 3
CH-8092 Zurich, Switzerland
Email: plesko@lem.ee.ethz.ch

***Abstract*—Cost, volume and weight are three major driving forces in the automotive area. This is also true for hybrid electric vehicles, which attract more and more attention due to increasing fuel costs and pollution.**

Since the energy distribution system causes a significant share of the volume/costs, a new concept for integrating dc-dc converters, which transfer the power between the low- and high-voltage buses, in the inverter/drive system is presented in this paper. There, the basic operation principle, analytical design equations and control strategies for improving the efficiency are explained. These considerations are validated by simulations and measurements.

I. Introduction

Hybrid electric vehicles are attracting more and more interest. Growing fuel costs and environmental concerns are just two factors that push the research activities in this area, and there are many car manufacturers that develop hybrid vehicles. There exist various possibilities for the set up of the electric power system of a hybrid vehicle, but the basic structure often has voltage levels and interconnections as shown in Figure 1.

Conventionally, hybrid electric vehicles have two different voltage levels. A 12 V battery supplies a 14 V dc bus over a battery charge/discharge unit. Traditional loads such as a heater, audio and lighting systems are supplied by this low-voltage bus.

Due to the high power levels the propulsion system is connected to a high-voltage 200 V...600 V dc bus for increasing the efficiency, whereas the supply voltages of the electric machine are generated by a dc-ac converter connected to this high-voltage bus. The low- and the high-voltage bus are interconnected bidirectionally via a dc-dc converter, which needs to be galvanically isolated for safety reasons.

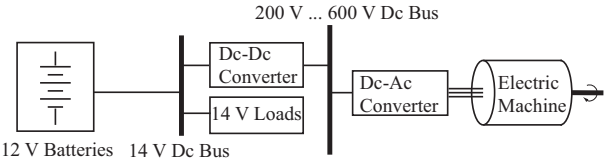

Figure 1: A typical possibility of a conventional electrical power distribution system architecture for hybrid electric vehicles.

Also in conventional cars, industry considered the introduction of an additional 42 V dc bus powered by a 36 V battery due to the growing number of electrical loads. There, the 200 V to 600 V high-voltage level could be omitted and the propulsion system could be supplied with 42 V. In [1] this system is compared to the conventional one. Basically, also other combinations are possible, but the advantages of the high-voltage solution outweigh those of the 42 V system. Therefore, it is assumed in the following that the propulsion system is fed via a 200 V to 600 V high-voltage bus.

To increase the power density and reduce the costs of the electric system, the dc-dc converter, interconnecting the low- and high-voltage buses, could be functionally integrated into the inverter/machine. For example, in [2] a possible integration of the dc-dc converter in the inverter system is presented, but it is applicable only for two split-phase motors. Another integration possibility is described in [3], which is, however, not galvanically isolated.

This concept, however, does not provide galvanic isolation, which is required for safety reasons as already mentioned above. In addition, the output voltage V_{out} of the dc-dc converter cannot be controlled in every operation region of the drive system. If the inverter operates for example in the six-step mode, the switching states of the inverter are completely determined. Consequently, there is no degree of freedom for controlling the output voltage of the dc-dc converter.

To solve these problems, an integrated high-voltage to low-voltage dc-dc converter with galvanic isolation is proposed in this paper. Depending on the actual distribution system, this converter can be used to convert 200...600 V to 14 V or 42 V bidirectionally.

The starting point for the following considerations is a conventional full-bridge converter feeding a high-frequency transformer (see Figure 2(a) - DAB), whose high-frequency output is rectified to the output voltage V_{out}. The secondary-side rectifier could be a conventional full-bridge configuration,

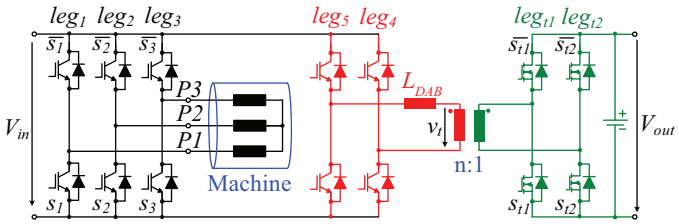

(a) Separated dc-dc converter and inverter

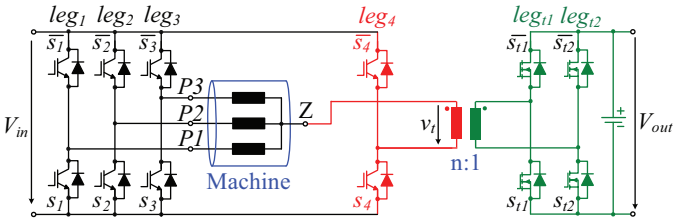

(b) Proposed integrated dc-dc converter: MFCS-I

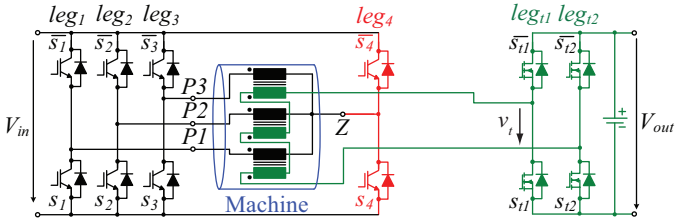

(c) Proposed integrated dc-dc converter: MFCS-II

Figure 2: Multi Functional Converter Systems (MFCS).

or a diode rectifier, in case only unipolar power transfer is required.

In a first step, the fifth leg (i.e. leg_5 in Figure 2(a)) of the conventional system is replaced by the zero-sequence voltage of the inverter. There, the transformer is connected between the star point and the midpoint of the primary-side leg four (see Figure 2(b)). This concept is referred to as Multi Functional Converter System I (MFCS-I) [4] in the following.

In a second step, the iron core of the motor could be used for integrating the transformer as shown in Figure 2(c). Compared to the conventional machine, there is an additional secondary winding for each phase. As these secondary windings are connected in series, the total voltage appearing on the secondary side is proportional to the zero-sequence voltage of the machine in the no-load case. Section II gives a more detailed report of this concept, referred to as Multi Functional Converter System II (MFCS-II) [5]. Other possibilities to use the iron core of the motor or the input inverter for integrating the transformer are presented in [6] and [7]. However, the concept presented in this paper offers a higher power density because it does not need a three-phase rectifier.

In this paper, the basic function of the second variant (MFCS-II) is explained and simulation as well as experimental results are presented. Furthermore, the basic operation principle of the MFCS-II is explained in **Subsection II-A**, followed

Figure 3: Simplified schematic of the integrated transformer, where the motor windings are used as primary windings and the stator iron as core.

by a more detailed analysis in **Subsection II-B**, where also different control and switching strategies are proposed. The simulation results presented in **Subsection II-C** validates the analytical model. The theoretical results are verified experimentally by means of a 10 kW prototype in **Subsection II-D**. In **Section III**, the MFCS-II is compared to the first variant, the multi functional converter system I (MFCS-I).

II. MFCS-II

In the MFCS-II, the galvanic isolation of V_{out} is integrated into the motor (see Figure 2c) in order to reduce the costs and the weight compared to the conventional system and the MFCS-I. To do so, a small number of additional windings with relatively small cross section must be placed in the slots together with the conventional motor windings.

This section starts with an explanation of the basic operation principle of the MFCS-II by studying the zero-sequence voltage and introducing an equivalent circuit for the dc-dc converter. After discussing the control in subsection II-B and presenting simulation results in subsection II-C, measurement results are provided in subsection II-D.

A. *Basic Operation Principle – MFCS-II*

Both concepts MFCS-I and MFCS-II are based on the utilization of the zero-sequence voltage, whose definition and calculation are well known. The zero-sequence voltage related to the negative bus bar can be calculated as

$$v_z = \frac{V_{in}}{3}(\overline{s_1} + \overline{s_2} + \overline{s_3}),$$

where $\overline{s_\nu} = 1$ if switch $\overline{s_\nu}$ is closed and switch s_ν open and $\overline{s_\nu} = 0$ if $\overline{s_\nu}$ is open and s_ν closed (see Figure 2). Furthermore, V_{in} denotes the input voltage.

In Figure 3 a simplified sketch of the transformer winding integration used in the MFCS-II is shown. The conventional motor windings act as the primary windings of the three transformers. The additional windings are the secondary ones. The machine stator iron is also used as transformer core.

Figure 4 shows the general equivalent circuit of the motor with integrated transformer, which will be explained in the following. First, it is assumed for simplicity that the machine is not rotating. If a voltage is applied to phase $P1$, a flux Ψ_{P1} begins to build up, inducing a voltage v_{P1_2} in the secondary winding $P1_2$, which is proportional to v_{P1_1} (ignoring losses). If the machine is rotating, the rotor additionally induces the

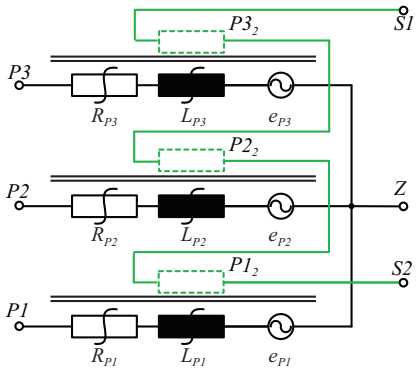

Figure 4: Equivalent circuit of the motor with integrated transformer. Details of each phase are shown in Figure 5.

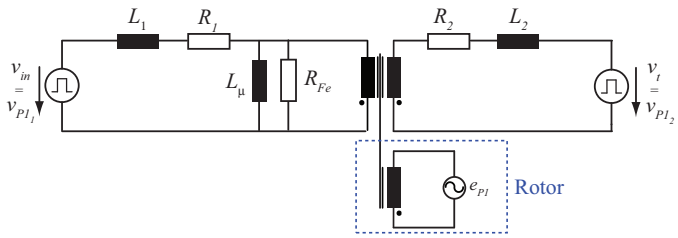

Figure 5: Equivalent circuit of one phase, where v_{in} is the output voltage of the inverter, e_{P1} the back EMF of the motor, which induces a voltage in the motor/primary winding as well as in the secondary winding and v_t denotes the rectifier voltage.

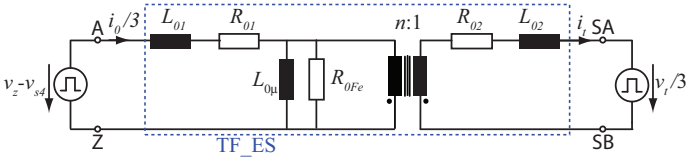

Figure 6: Zero-sequence equivalent circuit of the dc-dc converter based on simplifying the equivalent circuit shown in Figure 5.

voltage e_{P1} in phase $P1$. The same applies to phases $P2$ and $P3$. Each phase of the motor with the additional transformer winding can therefore be represented by the transformer equivalent circuit presented in Figure 5.

If the secondary windings are connected in series, the voltages induced by the rotor add up zero since they are zero-sequence free. Moreover, also the induced phase voltages are connected in series on the secondary side, so that only the zero-sequence voltage remains there. Consequently, the equivalent circuit of the integrated dc-dc converter could be simplified to Figure 6. At the input side the voltage $v_{in} = v_z - v_{s4}$, consisting of the zero sequence voltage v_z of the converter as defined in (1) and the voltage v_{s4} generated with the fourth converter leg, must be considered.

In the equivalent circuit in Figure 6 the three main inductances of the motor (cf. L_m in Figure 12) are not included since the flux in these inductances cancels out due to the spatial arrangement in case the windings are excited with a zero-sequence current. Furthermore, the winding resistances of the integrated transformer are denoted by R_1 and R_2, the leakage inductances by L_1 and L_2, the iron resistance by R_{Fe} and the main inductance of the transformer by L_μ. Voltage v_t represents the rectifier voltage (see Figure 2(c)).

It is important to note that the real and the imaginary part of the equivalent circuit's impedance measured between the points A and Z with no load on the secondary side correspond to the phase resistance and the stray inductance found in the conventional motor's equivalent circuit [8].

By integrating the dc-dc converter the flux in the machine is increased due to magnetizing current of the integrated transformer. Since the power level of the dc-dc converter is intended to be much smaller than the machine power, this additional flux is small compared to the conventional flux without integrated transformer and does not impair the normal motor operation. Nevertheless, to keep this additional flux small and prevent the iron from saturating also for the six-step mode proper pulsing of s_4 and $\overline{s_4}$ is required.

The presented system is similar to a Dual Active Bridge converter (DAB) [9]. There, the inductance between the two H-bridges could either be built as a discrete inductance (L_{DAB} in Figure 2(a)) or it could be implemented as the transformer's stray inductance provided that it is large enough. In the MFCS-II, the stray inductance of the integrated transformer acts as the DAB inductance, but as the voltage v_z at the input of the system is neither average free (related to the switching frequency) nor free from even harmonics, conventional modulation schemes used for DABs cannot be applied.

In the MFCS-II, the secondary H-bridge is used as active rectifier in order to guarantee that the voltage time product across the integrated transformer remains below a predetermined level. An unidirectional implementation with a diode rectifier would be also possible, but in order to limit the additional flux in the motor, a special control must be utilized.

B. *Control Schemes for MFCS-II*

For obtaining a stable output voltage a new control scheme for the fourth leg and the active rectifier is required. This modulation scheme has to be guaranteed that

- the transformer does not saturate (Condition I) and
- the desired power is transferred (Condition II).

1) Condition I - Flux Balance: The first condition is equivalent to applying a local average free voltage to the transformer windings. Therefore, the relative off time δ_{s4} of s_{s4} is determined by the relative off times of the three inverter switches as

$$\delta_{s4} = \frac{1}{3}(\delta_{s1} + \delta_{s2} + \delta_{s3})$$

as the switching period average of the zero-sequence voltage is not always $\frac{V_{in}}{2}$ related to the negative bus bar but may

depend on the motor's electrical angle ωt. Consequently, the only degree of freedom on the primary side is the relative time offset between the zero phase voltage and the fourth leg voltage, represented by the angle φ_{s4} (see Figure 7).

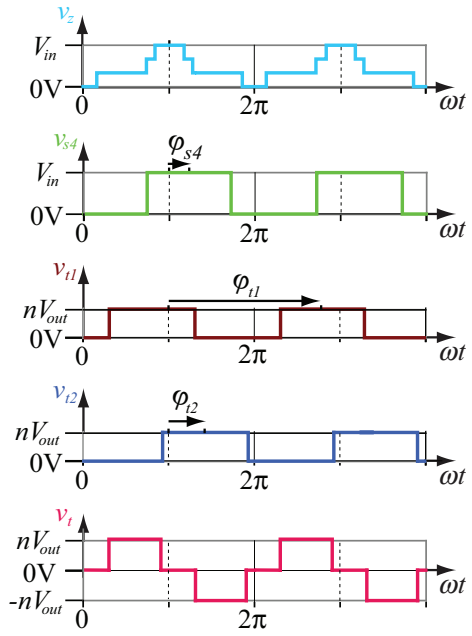

Figure 7: Converter waveforms: zero sequence voltage v_z, voltage v_{s4} across s_4 ,voltage v_{t1} across s_{t1}, voltage v_{t2} across s_{t2} and transformer voltage v_t

To guarantee a local average free voltage on the secondary side, the switching state $s_{t1} = 1, s_{t2} = 0$ must have the same on time during a switching period as the state $s_{t1} = 0, s_{t2} = 1$, i.e. the switching states $s_{t1} = 0, s_{t2} = 0$ and $s_{t1} = 1, s_{t2} = 1$ do not influence the average voltage. Assuming just one switching cycle per period, there are (at most) four possible switching schemes for a given transformer voltage, which differ only in the free-wheeling period $s_{t1} = 0, s_{t2} = 0$ and $s_{t1} = 1, s_{t2} = 1$ (cf. Figure 8). Evidently, the conduction losses are the same. As the same is true for the switching losses, the four schemes are equivalent.

For simplicity, only last two schemes are discussed in the following, which are comparable to a phase shift modulation, i.e. the relative on time of s_{t1} and s_{t2} is 50 percent. Then the only degree of freedom for each leg is the relative time offset between the zero phase voltage and the active rectifier leg voltage, represented by the angle φ_{t1} and φ_{t2} respectively (cf. Figure 7).

2) Condition II - Transferred Power: To calculate the transferred power, the Fourier series of the three voltages v_z, v_{s4} and $\frac{v_t}{3}$ with the switching frequency f_{sw} can be described

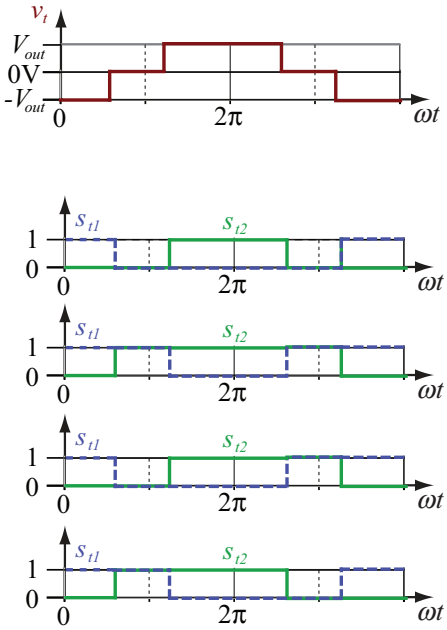

Figure 8: The four equivalent switching schemes for a given local average free transformer voltage

as

$$
\begin{aligned}
v_z &= a_{z(0)} + \sum_{k=1}^{\infty} a_{z(k)} \cos(k\omega_{sw} t) \\
v_{s4} &= a_{s4(0)} + \sum_{k=1}^{\infty} a_{s4(k)} \cos(k\omega_{sw} t - k\varphi_{s4}) \\
\frac{v_t}{3} &= \sum_{k=1}^{\infty} a_{t(k)} [\cos(k\omega_{sw} t - k\varphi_{t1}) - \cos(k\omega_{sw} t - k\varphi_{t2})]
\end{aligned}
$$

where $\omega_{sw} = 2\pi f_{sw}$ and

$$
a_{z(k)} = \begin{cases} -\frac{2V_{in}}{3k\pi}[sin(k\pi\delta_a) + sin(k\pi\delta_b) + sin(k\pi\delta_c)] & \text{if } k \text{ odd} \\ \frac{2V_{in}}{3k\pi}[sin(k\pi\delta_a) + sin(k\pi\delta_b) + sin(k\pi\delta_c)] & \text{if } k \text{ even} \end{cases}
$$

$$
a_{s4(k)} = \begin{cases} -\frac{2V_{in}}{k\pi} sin(k\pi\delta_{s4}) & \text{if } k \text{ odd} \\ \frac{2V_{in}}{k\pi} sin(k\pi\delta_{s4}) & \text{if } k \text{ even} \end{cases}
$$

$$
a_{t(k)} = \begin{cases} -\frac{2nV_{out}}{3k\pi} & \text{if } k \text{ odd} \\ 0 & \text{if } k \text{ even} \end{cases}
$$

As the system in Figure 6 is an LTI system, the steady-state current can be splittend into the part i_{tvzs4} generated by $v_z - v_{s4}$ and the part i_{tvt} generated by v_t, i.e. $i_t = i_{tvzs4} + i_{tvt}$. These currents can be calculated by

$$
\begin{aligned}
i_{tvzs4} &= \frac{v_z - v_{s4}}{Z_0} \\
&= \sum_{k=1}^{\infty} |G(jk\omega_{sw})| \{ a_{z(k)} \cos(k\omega_{sw} t + \angle G(jk\omega_{sw})) \\
&\quad - a_{s4(k)} \cos(k\omega_{sw} t - k\varphi_{s4} + \angle G(jk\omega_{sw})) \\
&\quad - a_{t(k)} \cos(k\omega_{sw} t - k\varphi_{t1} + \angle G(jk\omega_{sw})) \\
&\quad + a_{t(k)} \cos(k\omega_{sw} t - k\varphi_{t2} + \angle G(jk\omega_{sw})) \},
\end{aligned}
$$

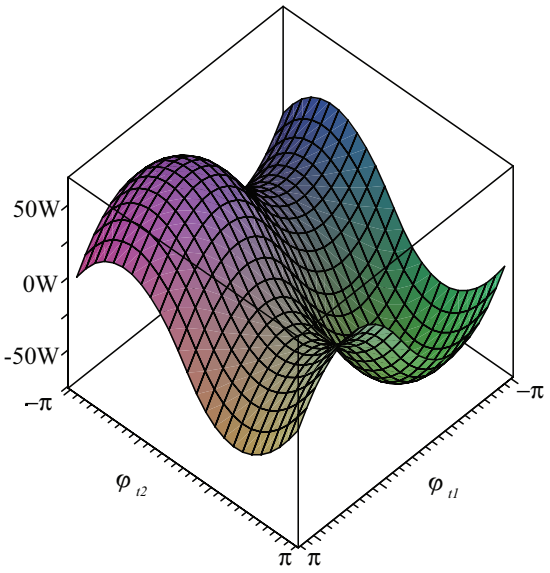

Figure 9: Transferable power in dependance of the phase shifts φ_{t1} and φ_{t2} for the test system. The phase shift φ_{s4} has been set to π, the input voltage to V_{in}=150 V, the output voltage to V_{out}=14 V and the motor speed to 150 rpmh.

where $G(jk\omega_{sw})$ is the transfer function from $v_z - v_{s4}$ to i_{tvzs4}, i.e. the impedance, at the frequency $\frac{k\omega_{sw}}{2\pi}$. Current i_{tvt} is calculated in analogue manner.

As the current, also the transferred steady-state power can be splittend since $p = 3\frac{v_t}{3} i_t = v_t i_{tvzs4} + v_t i_{tvt} = p_{tvzs4} + p_{tvt}$ with

$$\begin{aligned} p_{tvzs4} \quad = \quad & 3nV_{out} \sum_{k=1}^{\infty} \{ \frac{|G(jk\omega_{sw})|}{k\pi} 2 \sin\left(\frac{k\varphi_{t1} - k\varphi_{t2}}{2}\right) \\ & [a_{z(k)} \sin\left(\frac{k\varphi_{t1} + k\varphi_{t2}}{2} + \angle G(jk\omega_{sw})\right) \\ & -a_{s4(k)} \sin\left(\frac{k\varphi_{t1} + k\varphi_{t2}}{2} - k\varphi_{s4} + \angle G(jk\omega_{sw})\right) \\ & -a_{t(k)} \sin\left(\frac{k\varphi_{t1} + k\varphi_{t2}}{2} - k\varphi_{t1} + \angle G(jk\omega_{sw})\right) \\ & +a_{t(k)} \sin\left(\frac{k\varphi_{t1} + k\varphi_{t2}}{2} - k\varphi_{t2} + \angle G(jk\omega_{sw})\right)] \}. \end{aligned} \tag{1}$$

The same applies to p_{tvt}.

3) Degrees of Freedom: As one of the three degrees of freedom $\varphi_{s4}, \varphi_{t1}$ and φ_{t2} is needed to guarantee the desired power transfer, there remain two degrees of freedom for optimization of the switching scheme. It is obvious that these two phase shifts may not be chosen entirely free, as the maximal transferrable power is influenced by all the phase shifts. Figure 9 clarifies this. The phase shift φ_{s4} has been set to π, because this choice leads to the maximal transferrable power. It is obvious that φ_{t1} and φ_{t2} are entirely determined in the maximum point. But if the power demand decreases, there are several combinations of φ_{t1} and φ_{t2}, allowing for efficiency optimization.

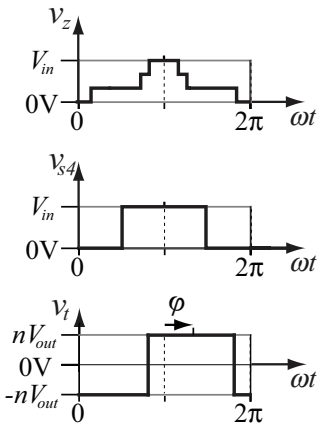

Figure 10: Converter waveforms: zero sequence voltage v_z, voltage v_{s4} across s_4 and rectifier voltage v_t for phase-shift modulation.

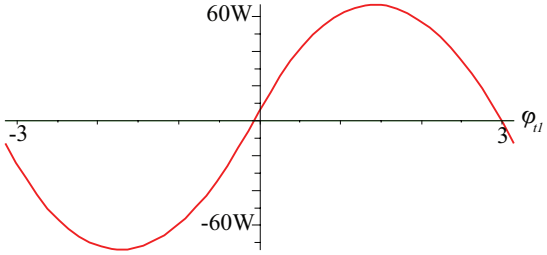

Figure 11: Transferable power with phase-shift in dependance of φ for the test system. The input voltage has been set to V_{in}=150 V, the output voltage to V_{out}=14 V and the motor speed to 150 rpmh

Since the MFCS-II is closely related to the Dual Active Bridge, the well known phase-shift modulation has also been implemented for this system. In phase-shift operation [9], the low voltage rectifier is controlled so that half the time the switches s_{t1} and $\overline{s_{t2}}$ are closed and the other half switches $\overline{s_{t1}}$ and s_{t2}. Furthermore, the voltage across the lower switch s_4 of the fourth leg leg_4 is controlled so that it is symmetrical with respect to π as depicted in Figure 10. There, the zero-sequence voltage v_z is used for the time and angle reference. The time/angle shift of the rectifier voltage v_t relating to the reference is refereed to as phase-shift φ.

As depicted in Figure 11, the transferred power can be influenced by the phase shift φ. Figure 11 can in fact be retrieved from Figure 9 by taking the $\varphi_{t2} = \varphi_{t1} + \pi$ cross section(s).

If the converter has to transfer the maximum power, there are practically no degrees of freedom, and the efficiency of the phase-shift modulation can hardly ever be increased (cf. Figure 9). However, when the power demand is decreased, the relative reactive power increases, thus decreasing the efficiency. There, an optimized switching scheme can improve the efficiency. For the simulated system with parameters as described in subsection II-C, the efficiency for transferred power of 500 W at 200 V input voltage can be increased from

61 percents for phase shift to 82 percents with an optimal switching strategy. There, the three degrees are optimized for minimal losses and the transferable power (1) is the constraint.

To improve the efficiency in low power operating points even more, it is possible to switch the switches of the fourth leg and/or the secondary side legs more often than the inverter switches. As the optimal switched currents are smaller for this modulation, the switching losses do not increase strongly or might even decrease. The improvement of the rms-currents decreases the conduction losses, thus decreasing the total losses for certain operating points. That is especially true for low power transfers. This modulation type will be presented in a future paper.

Table I summarizes the degrees of freedom to improve the efficiency. It has to be noted that one of the phase-shift angles is determined by the power demand, and the other controller degrees of freedom are not entirely free as explained before.

Table I: Degrees of freedom.

Controller degrees of freedom:

φ_{s4}: phase-shift angle of v_{s4}
φ_{t1}: phase-shift angle of v_{t1}
φ_{t2}: phase-shift angle of v_{t2}
Multiple switching

Additionally, an appropriate design of the converter's parameter, for example of the turn's ratio n, is very important for a good efficiency.

C. *Simulation of MFCS-II*

Based on the control scheme that was presented in the preceding section simulations of the model in Figure 2(c) were carried out. There, a PI-controller for controlling the phase-shift, a resistive load, and the machine model from Figure 12 have been assumed. In this figure the block TF_ES represents the zero-sequence equivalent circuit shown in Figure 6. The inductor L_m represents the main inductance of the machine, $e_{P\nu}$ the back EMF. As the components of the transformer's equivalent circuit are frequency dependent, the series connection of R_1 and L_1, R_2 and L_2 and the parallel connection of R_{Fe} and L_μ are modelled as ladder circuit's [8].

As the prototype machine described in section II-D has smaller power ratings than the target system, the zero sequence impedance of a machine designed for hybrid cars was measured. Based on this measurement the simulation parameters for the equivalent circuit in Figure 6 have been scaled based on the prototype's parameters.

With these assumptions and the parameters given in Table II the simulation results shown in Figure 13 have been obtained. There, it can be seen that the output voltage and thus the output power are constant over the period of the motor frequency. Furthermore, the voltage time product of the integrated transformer is below the desired level, so that saturation is avoided.

Based on measurements on the machine designed for hybrid cars an efficiency of the dc-to-dc conversion is predicted to be above 80 percent. Further improvement of the efficiency could be achieved by applying a new control scheme, which is part of the ongoing research.

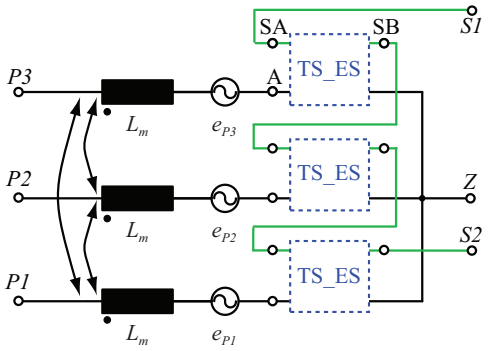

Figure 12: Model of the MFCS-II used for the simulations shown in Figure 13.

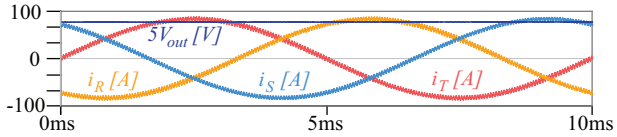

(a) Phase currents and output voltage

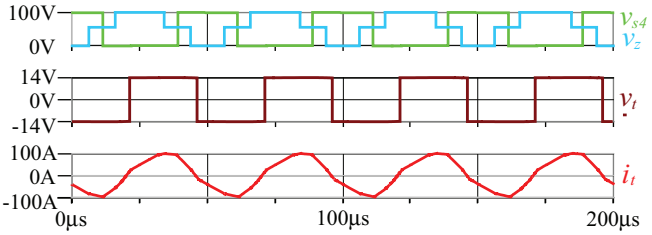

(b) Zoom: converter voltages (as introduced in Figure 6)

Figure 13: Simulation results for MFCS-II with parameters given in Table II.

Table II: Parameters of the MFCS.

Parameter	Value
nominal motor speed	1200 rpm
switching frequency f	20 kHz
input voltage V_{in}	200 V
output voltage V_{out}	14 V
maximum motor power	64 kW
simulated motor power	10 kW
nominal converter output power	1 kW
turns ratio n per phase	10

Table III: Parameters of the prototype.

Parameter	Value
number of poles	8
nominal speed	1500 rpm
input voltage V_{in}	250 V...400 V
motor power	3 kW
back EMFs e_R,e_S and e_T	67.8 Vrms at 1000 rpm

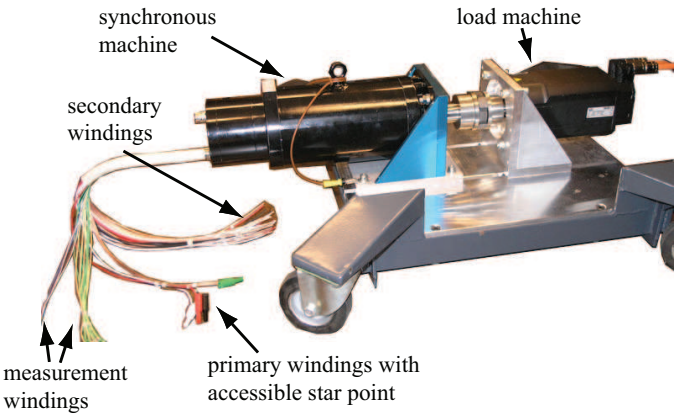

Figure 14: 3 kW permanent magnet synchronous motor with accessible star point (and secondary windings for MFCS-II).

D. Design and Experimental Results of MFCS-II

To verify the concept of the proposed MFCS-II, a synchronous motor with accessible star point and integrated secondary windings with the parameters given in Table III has been designed. Figure 14 shows the motor with the extra windings as described in subsection II-A.

The motor is driven by a 10 kW inverter, fed from an external dc-link voltage. Figure 15 shows the converter which includes the inverter, a fourth leg and a rectifier as shown in Figure 2(c).

The target system is assumed to include a 50 kW machine, the dc-dc converter having a nominal power of 1.5 kW and a maximum power of 5 kW. This leads for our 10 kW prototype machine to a dc-dc converter with a nominal power of 188 W and a maximum power of 1 kW.

Finally, the measurements in Figure 16 show the results for the operation of the MFCS-II. As the zero-sequence resistance of the investigated test machine is quite large only an efficiency of approximately 30 percent could be achieved. The large resistance value is caused by the fact that the machine is not intended for the use in automotive applications. Using an asynchronous motor, which is designed for parallel hybrid cars, a significantly lower resistance and efficiencies higher than 80% result (see section II-C). The machine rotates at 150 rpm with an input voltage of 150 V, transferring one third of the nominal power via the dc-dc converter. It is obvious that

Figure 15: Converter with the inverter, the fourth leg and the active rectifier.

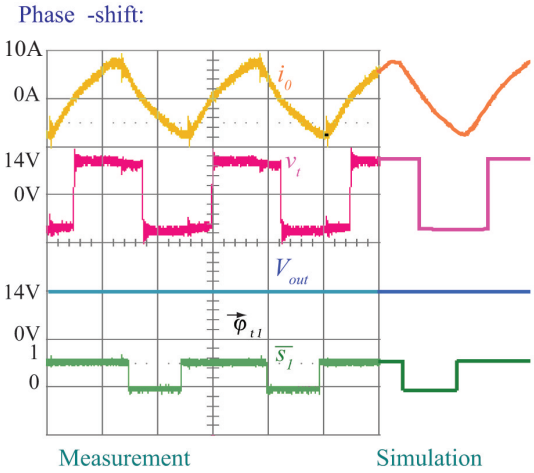

Figure 16: Measurement results obtained with the test system. There, the input voltage V_{in}=150 V, output voltage V_{out}=14 V, transferred power $p_{dc-dc} = 0.33 p_{dc-dc,nominal}$, rotational speed n=150 rpm.

it is possible to transfer power. Furthermore, the measurements agree very well with the simulations shown on the right hand side of Figure 16, which where performed with the model presented in section II-C.

III. Comparison of the MFCS-I and the MFCS-II

The measurements and simulations in the previous chapters showed that the MFCS-II works. In order to have an overview of the advantages and disadvantages of the proposed system, the MFCS-II is compared to the MFCS-I and the conventional Dual Active Bridge in this section.

As described in subsection II-A, the machine's zero-sequence inductance in the MFCS-I corresponds to the sum of the transformer stray and magnetizing inductance. Therefore, both the stray and the magnetizing inductance typically will

Table IV: Comparison of the conventional Dual Active Bridge, the MFCS-I and the MFCS-II.

DAB	**MFCS-I**	**MFCS-II**
4 legs	3 legs	3 legs
external transformer	external transformer	no external transformer
external inductance	no external inductance	no external inductance
conventional machine	machine with accessible star point	machine with accessible star point and additional windings
no additional flux	additional flux from zero-phase current	additional flux from magnetizing current
more components, but conventional machine	**less components, but accessible star point needed**	**the least components, but accessible star point and additional windings needed**

be smaller for the MFCS-II as for the MFCS-I, where the external transformer can be designed to meet the requirements. The small magnetizing inductance might increase the losses, depending on the operating point and the switching schemes. On the other hand, the MFCS-II machine sees only the flux generated by the magnetizing current, which is only a share of the zero-sequence current. Thus, the additional burden of the machine caused through the dc-dc converter is smaller in the MFCS-II, also leading to smaller magnetizing losses. With optimized switching strategies, the efficiencies of the two concepts are comparable. Of course, the Dual Active Bridge can be designed more easily for minimal losses, but if an optimized switching strategy and an appropriate motor is chosen for the MFCS's, its efficiency is similar to the conventional system.

An advantage of the MFCS-II is of course it's minimized number of components. The system saves not only one switch leg, as the MFCS-I, but also the external transformer. Besides the cost savings from the reduced number of components, the integration of the transformer can be accomplished by a supplier earlier in the production chain.

Table IV summarizes the comparison, where the number of legs is only applying to the DC/DC converter.

IV. Conclusion

By integrating the dc-dc converter, which connects the low and high-voltage buses of a hybrid vehicle, costs and weight of the hybrid propulsion system can be reduced. In this paper, a new concept for integrating the converter is presented which allows to replace one leg of the dc-dc converter by the inverter stage and to fully integrate the transformer in the machine.

Besides basic control structures and design equations new control schemes are be presented, which enable a significant improvement of the efficiency. For validating these considerations simulation and measurements results are presented, which show a good correspondence.

Based on the presented calculations an integrated drive system for a hybrid car with an efficiency of 80% is designed.

References

[1] A. Emadi, M. Ehsani, and J. Miller, "Advanced silicon rich automotive electrical power systems," in *Proc. 18th Digital Avionics Systems Conference*, vol. 2, 24-29 Oct. 1999, pp. 8.B.1–1–8.B.1–8.

[2] J. Wang, F. Peng, J. Anderson, A. Joseph, and R. Buffenbarger, "Low cost fuel cell converter system for residential power generation," *IEEE Transactions on Power Electronics*, vol. 19, no. 5, pp. 1315–1322, 2004.

[3] K. Moriya, H. Nakai, Y. Inaguma, H. Ohtani, and S. Sasaki, "A novel multi-functional converter system equipped with input voltage regulation and current ripple suppression," in *Conference Record of the 2005 Industry Applications Conference Fourtieth IAS Annual Meeting*, vol. 3, 2-6 Oct. 2005, pp. 1636–1642.

[4] H. Plesko, J. Biela, and J. W. Kolar, "Drehstromantriebssystem mit hochfrequent potentialgetrennter bidirektionalen Kopplung der Versorgungsspannungen," Patent 01 220/06, 2006.

[5] J. Biela, H. Plesko, and J. W. Kolar, "Drehstromantriebssystem mit motorintegriertem Hochfrequenztrafo zur bidirektionalen Kopplung der Versorgungsspannungen," Patent 01 219/06, 2006.

[6] J. M. Nagashima, D. S. Carlson, C. C. Stancu, S. Hit, and K. M. Rahman, "Auxiliary power conversion by phase-controlled rectification," Patent 6 617 820, September, 2003. [Online]. Available: http://www.freepatentsonline.com/6617820.html

[7] C. C. Stancu, S. Hiti, and J. Nagashima, "Auxiliary power conversion for an electric vehicle using high frequency injection into a pwm inverter," Patent 6 262 896, July, 2001. [Online]. Available: http://www.freepatentsonline.com/6262896.html

[8] H. Plesko, J. Biela, J. Luomi, and J. W. Kolar, "Novel concepts for integrating the electric drive and auxiliary dc-dc converter for hybrid vehicles," in *Twenty Second Annual IEEE Applied Power Electronics Conference, APEC 2007*, Feb. 2007, pp. 1025–1031.

[9] M. Kheraluwala, R. Gasgoigne, D. Divan, and E. Bauman, "Performance characterization of a high power dual active bridge dc/dc converter," in *Conference Record of the 1990 IEEE Industry Applications Society Annual Meeting*, vol. 2, 7-12 Oct. 1990, pp. 1267–1273.